On the simultaneous reconstruction of two space dependent coefficients in acoustic nonlinearity parameter tomography

Barbara Kaltenbacher* William Rundell†

Abstract

This paper considers the Westervelt equation, one of the most widely used models in nonlinear acoustics, and seeks to recover two spatially-dependent parameters of physical importance from time-trace boundary measurements. Specifically, these are the nonlinearity parameter $\kappa(x)$ often referred to as B/A in the acoustics literature and the wave speed $c_0(x)$. The determination of the spatial change in these quantities can be used as a means of imaging. We consider identifiability from one or two boundary measurements as relevant in these applications. For a reformulation of the problem in terms of the squared slowness $\mathfrak{s} = 1/c_0^2$ and the combined coefficient $\eta = \frac{\kappa}{c_0^2}$ we devise a frozen Newton method and prove its convergence. The effectiveness (and limitations) of this iterative scheme are demonstrated by numerical examples.

Keywords: nonlinearity parameter tomography, damped nonlinear wave equation, ultrasound.

ams classification: 35R30, 35R11, 35L70, 78A46

1 Introduction

Imaging with ultrasound has a long and successful history based on a vast range of applications. However, as is often the case, the use of lower frequencies naturally leads to lower resolution and at higher frequencies sound propagation is affected by scattering and stronger attenuation. Enhanced ultrasound-based techniques such as nonlinearity parameter imaging [5, 6, 8, 17, 33, 35, 38, 39], harmonic imaging [3, 34, 35], and vibro-acoustography [11, 12, 23, 30, 31] have been developed to overcome these drawbacks and improve imaging quality. They make use of *nonlinear effects* that arise at higher intensities or when waves interact and are characterised by a multiplicative coefficient that is usually called parameter of nonlinearity and denoted by B/A. We will here use the mathematically

*Department of Mathematics, Alpen-Adria-Universität Klagenfurt. barbara.kaltenbacher@aau.at.
†Department of Mathematics, Texas A&M University, Texas 77843. rundell@math.tamu.edu

convenient abbreviation[s] κ for a quantity containing B/A. This coefficient depends on tissue properties and therefore varies in the spatial direction, $\kappa = \kappa(x)$.

While ultrasound imaging relies on the propagation of sound waves and is therefore physically and mathematically correctly described by some wave-type partial differential equation (PDE), algorithms implemented in modern ultrasound scanners make use of model simplifications that allow one to apply methods from signal processing (beamforming, filtering) to generate an image based on the principles of transmission and reflection, based on differences in the acoustic impedance Z. These simplifications are not able to capture nonlinearity so that one has to return to the PDE model and consider $\kappa = \kappa(x)$ (and often also the speed of sound $c_0 = c_0(x)$) as a spatially variable coefficient.

In the following subsections we provide more background on the mathematical models. In particular we will show at which position in the PDE these coefficients appear, which of course is a factor crucial for their recovery. We then describe the inverse problem and the basic method of its solution.

We consider, as one of the most established classical model of nonlinear acoustics, the Westervelt equation in pressure formulation

$$u_{tt} - c_0^2 \Delta u - b\Delta u_t = \kappa (u^2)_{tt} + g \text{ in } (0,T) \times \Omega\,, \tag{1}$$

where u is the acoustic pressure, c_0 the speed of sound, b the diffusivity of sound, ϱ_0 the mass density, and $\kappa = \frac{\beta_a}{\varrho_0 c_0^2} = \frac{1}{\varrho_0 c_0^2}(\frac{B}{2A} + 1)$ contains the nonlinearity parameter β_a or B/A. [1] We assume (1) to hold in a domain $\Omega \subseteq \mathbb{R}^3$ and equip it with initial conditions $u(t=0) = u_0$, $u_t(t=0) = u_1$, as well as absorbing or impedance boundary conditions on the rest of the boundary to enable restriction to a bounded computational domain Ω, which without loss of generality we can assume to be smooth. The space- and time-dependent interior source term g in (1) models excitation by a piezoelectric transducer array.

The pressure data h taken at the receiver array is expressed as a Dirichlet trace on some manifold Σ immersed in the computational domain Ω or attached to its boundary $\Sigma \in \overline{\Omega}$

$$h(t,x) = u(t,x), \quad (t,x) \in (0,T) \times \Sigma. \tag{2}$$

Note that Σ could [may as well just] simply be a subset of discrete points on a manifold.

The inverse problem of nonlinearity parameter tomography consists of reconstructing $\kappa = \kappa(x)$ from measurements (2). Often, the speed of sound varies in space as well $c_0 = c_0(x)$ and needs to be recovered alongside with κ. This is a natural requirement as the sound speed will between objects to be imaged and also from the background.

Reconstruction of $c_0 = c_0(x)$ as a PDE coefficient is actually already being done in ultrasound tomography [2, 13, 14, 18, 32] for c_0, but in a linear wave equation, that is, with

[1] More precisely, the PDE is $\frac{1}{\lambda(x)} u_{tt} - \nabla \cdot (\frac{1}{\varrho_0(x)} \nabla u) - bDu = \kappa (u^2)_{tt} + g$ with u being the pressure, λ the bulk modulus, ϱ_0 the mass density, and $c_0 = \frac{\lambda}{\varrho_0}$ the sound speed, (cf., e.g., [4, 28] for the linear case). As mentioned above, spatial variability of ϱ is not relevant in our context; rather, dependence of c_0 on x is due to variability of λ.

$\kappa = 0$. We mention in passing that in principle the mass density ϱ_0 also varies in the spatial direction. However, in ultrasound imaging, this coefficient does not play a significant role and is therefore usually neglected.[2]

We refer to [1, 24, 25, 37] for results related to the identification of the nonlinearity coefficient κ alone. In [1] its uniqueness from the whole Neumann-Dirichlet map (instead of the single measurement (2)) is shown; [37] provides a uniqueness and conditional stability result for the linearised problem of identifying κ in a higher order model of nonlinear acoustics in place of the Westervelt equation. In [24, 25] we have proven injectivity of the linearised forward operator mapping κ to h in the Westervelt equation with classical strong damping and also with some fractional damping models as relevant in ultrasonics.

The aim of this paper is to provide results on the *simultaneous* recovery of $\kappa(x)$ and $c_0(x)$. In Section 2 we will prove injectivity of the linearised forward operator from measurements with two excitations. This serves as a basis for applying a frozen Newton method and showing its convergence in Section 3.1. Numerical reconstruction results are provided in Section 3.2.

1.1 The inverse problem

Consider identification of the space dependent nonlinearity coefficient $\kappa(x)$ and sound speed $c_0(x)$ for the attenuated Westervelt equation in pressure form

$$\begin{aligned} \big(u - \kappa(x)u^2\big)_{tt} - c_0(x)^2 \triangle u + D[u] = r \quad &\text{in } \Omega \times (0,T) \\ \partial_\nu u + \gamma u = 0 \text{ on } \partial\Omega \times (0,T), \quad u(0) = 0, \quad u_t(0) = 0 \quad &\text{in } \Omega \end{aligned} \tag{3}$$

from observations of the acoustic pressure

$$h(x,t) = u(x,t)\,, \quad x \in \Sigma\,, \quad t \in (0,T). \tag{4}$$

The physical meanings of the quantities in this model are listed in Table 1, where we assume $\varrho_0 > 0$, $b > 0$, $\gamma \geq 0$ to be known constants, whereas B/A (and therefor κ), as well as c_0 may depend on the x variables.

In equation (3), the damping term D is defined by one of the two following fractional damping models

$D = b(-\triangle)^\beta \partial_t^\alpha$ (combination of Caputo-Wismer-Kelvin and Chen-Holm – CH)

$D = b_1(-\triangle)\partial_t^{\alpha_1} + b_2\partial_t^{\alpha_2+2}$ (fractional Zener – FZ)

[2]The notation c_0, ϱ_0 for the (reference) sound speed and mass density, respectively, refers to he usual decomposition of the mass density into a reference and a fluctuation part $\varrho = \varrho_0 + \varrho_\sim$, and correspondingly for $c_0 = \frac{\lambda}{\varrho_0}$, where λ is the bulk modulus. While the total mass density ϱ would be subject to a balance law (namely conservation of mass) and thus appear as one of the states in a PDE model, its appearance as a coefficient only affects the reference part ϱ_0. This is due to the typical expansion rules (known as Blackstock's scheme in the nonlinear acoustics literature) for obtaining linear and quadratic acoustic wave equations from nonlinear balance and constitutive laws, cf. e.g., [15, 20] and the references therein.

u ... pressure $[gm^{-1}s^{-2}]$
c_0 ... sound speed $[m\,s^{-1}]$
$\kappa = \frac{B/A+2}{\varrho_0 c_0^2}$ ... nonlinearity coefficient $[g^{-1}\,m\,s^2]$
$\varrho_0 \in \mathbb{R}^+$ ... mass density $[g\,m^{-3}]$
B/A ... nonlinearity parameter $[1]$
$b \in \mathbb{R}^+$ ... diffusivity of sound $[m^2\,s^{-1}]$
$\gamma \in \mathbb{R}_0^+$ ... boundary impedance $[m^{-1}]$

Table 1: Physical quantities appearing in the PDEs.

(for more details see, e.g., [25] and the references therein, in particular [9, 36, 10] for CH and [16, 29, 7] for FZ).
The time fractional derivatives appearing in the damping models are defined by the Djrbashian-Caputo derivative

$$\partial_t^\alpha u = I^{1-\alpha} u_t$$

with the Abel integral operator

$$(I^{1-\alpha} v)(t) \frac{1}{\Gamma(1-\alpha)} \int_0^t \frac{v(s)}{(t-s)^\alpha}\, ds$$

and $\alpha \in (0,1)$. For defining fractional powers of the negative Laplacian $-\triangle$ with impedance boundary conditions in the CH case, we use the spectral definition

$$((-\triangle)^\beta v)(x) = \sum_{j=1}^{\infty} \lambda_j^\beta \sum_{k \in K^{\lambda_j}} \langle v, \varphi_j^k \rangle \varphi_j^k(x).$$

Excitation is modeled by an interior space and time dependent source term r, which indeed allows to describe the acoustic signal emitted by a transducer array immersed in the domain Ω, see also [21].

In most of this paper, we will work with the following alternative formulation that moves the spatially variable coefficient $c_0(x)$ away from the Laplacian and thus leads to a symmetric positive (as well as relatively simple) elliptic differential operator in the equation. [3] To this end, we divide (3) by $c_0^2(x)$ and rewrite it, using the new coefficient functions $\mathfrak{s}(x)$, $\eta(x)$, as

$$\begin{aligned} &\big(\mathfrak{s}(x)u - \eta(x)u^2\big)_{tt} - \triangle u + \tilde{D}u = \tilde{r} && \text{in } \Omega \times (0,T) \\ &\partial_\nu u + \gamma u = 0 \text{ on } \partial\Omega \times (0,T), \quad u(0) = 0, \quad u_t(0) = 0 && \text{in } \Omega \end{aligned} \tag{5}$$

[3] An alternative to achieve symmetry would be to use the weighted L^2 inner product with weight function $1/c_0^2(x)$

where (again with physical units in brackets)

$\mathfrak{s} = \frac{1}{c_0^2} \dots$ squared slowness $[m^{-2}s^2]$

$\eta = \frac{\kappa}{c_0^2} = \frac{\beta_a}{\varrho_0 c_0^4} = \frac{B/A+2}{\varrho_0 c_0^4} = \frac{B/A+2}{\varrho_0}\mathfrak{s}^2 \dots$ nonlinearity coefficient $[g^{-1}m^{-1}s^4]$

$\tilde{D} = \tilde{b}(-\triangle)^\beta \partial_t^\alpha$ (CH) or $\tilde{D} = \tilde{b}_1(-\triangle)\partial_t^{\alpha_1} + \tilde{b}_2\partial_t^{\alpha_2+2}$ (FZ).

Note that we neglect variability of the damping and driving terms term with division by $c_0(x)^2$ and assume $\tilde{D}$ to come with constant and known coefficients; incorporation of this $c_0(x)$ dependence would lead to the PDE

$$\big(\mathfrak{s}(x)u - \eta(x)u^2\big)_{tt} - \triangle u + \mathfrak{s}\, Du = \mathfrak{s}\, r \quad \text{in } \Omega \times (0,T). \tag{6}$$

Neglecting this dependency in the damping term can be justified by smallness of the damping coefficient so that spatial variability of this term has a very minor effect. Neglecting spatial variability of $\mathfrak{s}$ in the excitation term does not matter due to the fact that the support of r is typically remote from the region of variable (and unknown) sound speed.

The inverse problem of reconstructing $\eta(x)$, $\mathfrak{s}(x)$ from the observations (4) can then be written as

$$F(\eta, \mathfrak{s}) = h, \tag{7}$$

where $F = C \circ S$ and with the parameter-to-state map $S : (\eta, \mathfrak{s}) \mapsto u$ where u solves (5) and is subject to the observation operator $C : u \mapsto \mathrm{tr}_\Sigma u$.

Well-definedness of the forward operator F and its linearisazion in appropriate function spaces is discussed at the beginning of Section 3.1.

Notation

Below we will make use of the spaces $\dot{H}^\beta(\Omega)$ induced by the norm

$$\|v\|_{H^\beta(\Omega)} = \Big(\sum_{j=1}^\infty \lambda_j^\beta \sum_{k \in K^{\lambda_j}} |\langle v, \varphi_j^k\rangle|^2\Big)^{1/2} \tag{8}$$

with the eigensystem (λ_j, φ_j) of some selfadjoint positive definite operator $\mathcal{A}$ (in this paper, it will be the negative Laplacian with impedance boundary conditions).

Moreover, the Bochner-Sobolev spaces $L^p(0,T;Z)$, $H^q(0,T;Z)$ with Z some Lebesgue or Sobolev spaces and T a finite or infinite time horizon will be used.

We denote the Laplace transform of a function $v \in L^1(0,\infty)$ by $\hat{v}(z) = \int_0^\infty e^{-zt}v(t)\,dt$ for all $z \in \mathbb{C}$ such that this integral exists.

2 Uniqueness

In this section we will prove linearised uniqueness of $\kappa(x)$ and $c_0(x)$ in $\mathbb{R}^d$ from two observations, considering the alternative formulation (5), with $T = \infty$ and

$$\mathfrak{s} = \frac{1}{c_0^2}, \quad \eta = \frac{\kappa}{c_0^2}. \tag{9}$$

To this end we will show injectivity of the linearised forward operator with respectto $\eta(x)$ and $\mathfrak{s}(x)$, given two appropriately chosen excitations $\tilde{r}_i$, $i \in \{1,2\}$. On the one hand, this is essential for well-definedness and convergence of the frozen Newton method considered in the reconstruction section below. On the other hand, via (9), uniqueness of $\eta(x)$ and $\mathfrak{s}(x)$ is equivalent to uniqueness of $\kappa(x)$ and $c_0(x)$.

The linearisation of the forward operator $F : (\eta, \mathfrak{s}) \mapsto \mathrm{tr}_\Sigma u$ is formally given by $F'(\eta,\mathfrak{s})(\underline{d\eta}, \underline{d\mathfrak{s}}) = \mathrm{tr}_\Sigma \underline{du}$, where $\underline{du}$ solves

$$\big(\mathfrak{s}(x)\,\underline{du} - 2\eta(x)\,u\underline{du}\big)_{tt} - \triangle \underline{du} + \tilde{D}\underline{du} = -\big(\underline{d\mathfrak{s}}(x)\,u - \underline{d\eta}(x)\,u^2\big)_{tt} \quad \text{in } \Omega \times (0,T). \tag{10}$$

This simplifies considerably if we linearise around vanishing nonlinearity $\eta = 0$ and constant wave speed $\mathfrak{s} = 1/c^2$ for some $c \in \mathbb{R}^+$, which yields $F'(0, \frac{1}{c^2})(\underline{d\eta}, \underline{d\mathfrak{s}}) = \mathrm{tr}_\Sigma \underline{du}$, where $\underline{du}$ solves

$$\frac{1}{c^2}\underline{du}_{tt} - \triangle \underline{du} + \tilde{D}\underline{du} = -\big(\underline{d\mathfrak{s}}(x)\,u^0 - \underline{d\eta}(x)\,(u^0)^2\big)_{tt} \text{ in } \Omega \times (0,T)$$

with homogeneous initial and boundary conditions. Here u^0 solves (5) with $\eta = 0$, $\mathfrak{s} = \frac{1}{c^2}$, which in its turn is a linear constant coefficient PDE.

To obtain injectivity of the linearisation, we use two excitations $\tilde{r}_i$, $i \in \{1,2\}$ and the corresponding components of the forward operator $\vec{F} = (F_1, F_2)$ are defined by $F_i = C \circ S_i$ with $S_i : (\eta, \mathfrak{s}) \mapsto u_i$ where u_i solves (5) with $\tilde{r} = \tilde{r}_i$, $i \in \{1,2\}$ and $C : u \mapsto \mathrm{tr}_\Sigma u$. Our goal is to prove that with an appropriate choice of $\tilde{r}_1$, $\tilde{r}_2$, the only solution to the homogeneous equation $\vec{F}'(0, \frac{1}{c^2})(\underline{d\eta}, \underline{d\mathfrak{s}}) = (0,0)$ is $(\underline{d\eta}, \underline{d\mathfrak{s}}) = (0,0)$. To this end, we construct the excitations $\tilde{r}_i$, $i \in \{1,2\}$ such that they lead to space-time separable solutions $u_i^0(x,t) = \phi_i(x)\psi_i(t)$ of (5),

$$\tilde{r}_i(x,t) := \frac{1}{c^2}\phi(x)\psi_i''(t) - \triangle\phi(x)\psi_i(t) + \tilde{D}[\phi\psi_i](x,t), \quad i \in \{1,2\}. \tag{11}$$

Expanding the solutions $\underline{du}_i$, $i \in \{1,2\}$ in terms of eigenfunctions φ_j of $-\triangle$, we can write the Laplace transformed solutions $\underline{du}_i$, $i \in \{1,2\}$ as

$$\widehat{\underline{du}_i}(x,z) = \sum_{j=1}^{\infty} \tfrac{1}{\omega_{\lambda_j}}(z) \sum_{k \in K^{\lambda_j}} \Big(\langle \underline{d\mathfrak{s}}\phi_i, \varphi_j^k \rangle \widehat{\psi_i''}(z) + \langle \underline{d\eta}\phi_i^2, \varphi_j^k \rangle \widehat{(\psi_i^2)''}(z) \Big) \varphi_j^k(x). \tag{12}$$

Here (λ_j, φ_j^k) is an eigensystem of $-\triangle$ equipped with the impedance boundary conditions of (5), $\langle \cdot, \cdot \rangle$ is the L^2 inner product on Ω, and

$$\omega_\lambda(z) = \begin{cases} \frac{1}{c^2}z^2 + \tilde{b}\lambda^\beta z^\alpha + \lambda \text{ for CH} \\ \tilde{b}_2 z^{2+\alpha_2} + \frac{1}{c^2}z^2 + \tilde{b}_1 \lambda z^{\alpha_1} + \lambda \text{ for FZ}, \end{cases}$$

are the reciprocals of the relaxation functions $\frac{1}{\omega_\lambda}$. We will make use of the following two auxiliary results on these relaxation functions.

Lemma 2.1 (Lemma 11.4 in [26]) *For* CH *or* FZ *damping, the poles of* $\frac{1}{\omega_\lambda}$ *differ for different* λ*.*

Lemma 2.2 (Lemma 11.5 in [26]) *For* CH *or* FZ *damping, the residues of the poles of* $\frac{1}{\omega_\lambda}$ *do no vanish.*

With (12), the premiss $F_i'(0, \frac{1}{c^2})(\underline{d\eta}, \underline{d\mathfrak{s}}) = 0$, $i \in \{1, 2\}$ reads as

$$0 = \sum_{j=1}^{\infty} \tfrac{1}{\omega_{\lambda_j}}(z) \sum_{k \in K^{\lambda_j}} \Big(\langle \underline{d\mathfrak{s}}\phi_i, \varphi_j^k \rangle \widehat{\psi_i''}(z) + \langle \underline{d\eta}\phi_i^2, \varphi_j^k \rangle \widehat{(\psi_i^2)''}(z) \Big) \varphi_j^k(x_0), \quad x_0 \in \Sigma \quad i \in \{1, 2\}.$$

Taking the residues at the singularities (which are the poles p_j of the relaxation functions) and applying Lemmas 2.1, 2.2, we can single out the contributions pertaining to the individual eigenvalues

$$0 = \sum_{k \in K^{\lambda_j}} \Big(\langle \underline{d\mathfrak{s}}\phi_i, \varphi_j^k \rangle \widehat{\psi_i''}(p_j) + \langle \underline{d\eta}\phi_i^2, \varphi_j^k \rangle \widehat{(\psi_i^2)''}(p_j) \Big) \varphi_j^k(x_0), \quad x_0 \in \Sigma \quad i \in \{1, 2\}, \quad j \in \mathbb{N}. \tag{13}$$

In case of one space dimension, the eigenvalues are single and the inner sum consists of one term $\#K^{\lambda_j} = 1$. However, in higher space dimensions, we typically have to deal with multidimensional eigenspaces, that is, $\#K^{\lambda_j} > 1$, with $(\varphi_j^k)_{k \in K^{\lambda_j}}$ as an orthonormal basis of the eigenspace corresponding to λ_j. Looking at each of these eigenspaces individually, it becomes apparent that in order not to lose the essential information separating the individual eigenfunction contributions contained in (13), we have to make the assumption that these eigenspaces keep their dimension after taking the observation traces. This can be cast as the linear independence assumption

$$\left(\sum_{k \in K^\lambda} b_k \varphi_k(x) = 0 \ \text{ for all } x \in \Sigma \right) \implies \big(b_k = 0 \text{ for all } k \in K^\lambda \big) \ . \tag{14}$$

for any eigenvalue λ of $-\triangle$ and is basically a geometric condition on Σ. Under condition (14), from (13) we immediately obtain

$$0 = \langle \underline{d\mathfrak{s}}\phi_i, \varphi_j^k \rangle \widehat{\psi_i''}(p_j) + \langle \underline{d\eta}\phi_i^2, \varphi_j^k \rangle \widehat{(\psi_i^2)''}(p_j), \quad j \in \mathbb{N}, \quad k \in K^{\lambda_j}, \quad i \in \{1, 2\}. \tag{15}$$

Now we set $\phi_1 = \phi_2 =: \phi$ for some function $\phi \neq 0$ almost everywhere in Ω, so that for each k and j, (15) becomes a two-by-two system of equations for the coefficients $a_j^k := \langle \underline{d\mathfrak{s}}\phi, \varphi_j^k \rangle$ and $b_j^k := \langle \underline{d\eta}\phi^2, \varphi_j^k \rangle$. Choosing ψ_1, ψ_2 such that for all poles p_j, the system matrix is regular, that is,

$$0 \neq \det \begin{pmatrix} \widehat{\psi_1''}(p_j) & \widehat{(\psi_1^2)''}(p_j) \\ \widehat{\psi_2''}(p_j) & \widehat{(\psi_2^2)''}(p_j) \end{pmatrix} \quad j \in \mathbb{N}, \tag{16}$$

we obtain $a_j^k = 0$, $b_j^k = 0$ for all $j \in \mathbb{N}$, $k \in K^{\lambda_j}$. Hence, the functions $\underline{d\mathfrak{s}}\,\phi$ and $\underline{d\eta}\,\phi^2$ vanish in $L^2(\Omega)$ and by our choice of $\phi \neq 0$ a.e. this implies that $\underline{d\mathfrak{s}} = 0$, $\underline{d\eta} = 0$ almost everywhere in Ω.

Thus, we have proven the following.

Theorem 2.1 *Assume that $T = \infty$, that (14) holds for the eigenspaces of $-\triangle$ and that the excitations $\tilde{r}_i$ take the form (11) with $\phi \in \mathcal{D}(-\triangle)$, $\phi \neq 0$ a.e. in Ω and ψ_1, ψ_2 satisfying (16). Then, $F_i'(0, \frac{1}{c^2})(\underline{d\eta}, \underline{d\mathfrak{s}}) = 0$, $i \in \{1, 2\}$ implies $\underline{d\eta} = 0$, $\underline{d\mathfrak{s}} = 0$.*

The same proof also works with the original $\kappa(x)$ and $c_0(x)$ formulation.

Indeed for $\tilde{F}_i : (\kappa, c_0^2) \mapsto \mathrm{tr}_\Sigma u_i$ (note that we take the *squared* sound speed as a variable), where u_i solves (3) with

$$r_i(x,t) := \phi(x)\psi_i''(t) - c_0^2 \triangle\phi(x)\psi_i(t) + D[\phi\psi_i](x,t), \quad i \in \{1,2\} \tag{17}$$

we get that the linearisation around vanishing nonlinearity coefficient $\kappa(x) = 0$ and constant sound speed $c_0^2(x) = c^2$ is $\tilde{F}_i'(0, c^2)(\underline{d\kappa}, \underline{dc_0^2}) = \mathrm{tr}_\Sigma \underline{du_i}$, where

$$\underline{du_i}_{,tt} - c^2 \triangle \underline{du_i} + D\underline{du_i} = \underline{d\kappa}\phi^2(\psi_i^2)'' + \underline{dc_0^2}\triangle\phi\psi_i \ \text{ in } \Omega \times (0,T).$$

Thus, from $\tilde{F}_i'(0, c^2)(\underline{d\kappa}, \underline{dc_0^2}) = 0$ for $i \in \{1, 2\}$, together with (14) and Lemmas 2.1, 2.2, we obtain, in place of (15), that

$$0 = \langle \underline{d\kappa}\phi, \varphi_j^k \rangle \widehat{(\psi_i^2)''}(p_j) + \langle \underline{dc_0^2}\triangle\phi_i^2, \varphi_j^k \rangle \widehat{\psi_i}(p_j), \quad j \in \mathbb{N}, \quad k \in K^{\lambda_j}, \quad i \in \{1,2\}.$$

Hence, under the assumption

$$0 \neq \det \begin{pmatrix} \widehat{(\psi_1^2)''}(p_j) & \widehat{\psi_1}(p_j) \\ \widehat{(\psi_2^2)''}(p_j) & \widehat{\psi_2}(p_j) \end{pmatrix} \quad j \in \mathbb{N}, \tag{18}$$

we obtain the following.

Theorem 2.2 *Assume that $T = \infty$, that (14) holds and the excitations r_i take the form (17) with $\phi \in \mathcal{D}(-\triangle)$, $\phi \neq 0$, $\triangle\phi \neq 0$ a.e. in Ω and ψ_1, ψ_2 satisfying (18). Then, $\tilde{F}_i'(0, c^2)(\underline{d\kappa}, \underline{dc_0^2}) = 0$, $i \in \{1, 2\}$ implies $\underline{d\kappa} = 0$, $\underline{dc_0^2} = 0$.*

3 Reconstruction of the nonlinearity coefficient and sound speed by a regularised Newton scheme

3.1 Well-definedeness and convergence a frozen Newton method

We first of all restrict ourselves to the classical Kelvin-Voigt damping $\tilde{D} = -\tilde{b}\triangle\partial_t$, that is, CH with $\alpha = \beta = 1$. Later on, in Subsection 3.1.1, we will return to both general damping models CH , FZ .

By a slight extension of [19, Theorem 1.1 and Proposition 3], the parameter-to-state map

$$S : \mathcal{D}(F) \to V := H^1(0,T;H^2(\Omega)) \cap W^{1,\infty}(0,T;H^1(\Omega)) \cap W^{2,\infty}(0,T;L^2(\Omega)) \tag{19}$$

is well-defined on

$$\mathcal{D}(F) := \{(\eta,\mathfrak{s}) \in L^\infty(\Omega)\times L^\infty(0,T;L^\infty(\Omega)) \,:\, \frac{1}{\mathfrak{s}} \in L^\infty(0,T;L^\infty(\Omega)),\ \mathfrak{s} \in H^1(0,T;L^3(\Omega))\}$$

for a smooth bounded domain $\Omega \subseteq \mathbb{R}^d$, $d \in \{1,2,3\}$, $\tilde{r} \in L^2(0,T;L^2(\Omega)) \cup H^1(0,T;H^{-1}(\Omega))$ with $\tilde{r}$ small enough in this norm. Note that we will have to deal with a potentially time-dependent $\mathfrak{s}$ below and thus consider a function space that is able to capture this. By Sobolev's Lemma, this implies that evaluation of u at single points or on a smooth manifold is feasible in a continuous way and thus $F : \mathcal{D}(F) \to Y$ is well-defined for any $Y \supseteq L^\infty(0,T;C(\Sigma))$ in case Σ is a smooth manifold or $Y \supseteq L^\infty(0,T;\ell^\infty(\Sigma))$ in case Σ is a set of discrete points. To make use of a Hilbert space structure, we will simply set $Y = L^2(0,T;L^2(\Sigma))$ or $Y = L^2(0,T;\ell^2(\Sigma))$, respectively.

Likewise it follows that for any $(\eta,\mathfrak{s}) \in \mathcal{D}(F)$, $(\underline{d\eta},\underline{d\mathfrak{s}}) \in L^\infty(\Omega) \times L^\infty(0,T;L^\infty(\Omega))$, the Gâteaux derivative of the forward operator is given by $F'(\eta,\mathfrak{s})(\underline{d\eta},\underline{d\mathfrak{s}}) = \mathrm{tr}_\Sigma \underline{du}$, where $\underline{du}$ solves (10).

In particular, for applying a frozen Newton method to (7), we linearise at $\mathfrak{s} = 1/c^2$ (for some constant c), $\eta = 0$, that is, we use $F'(0,1/c^2)(\underline{d\eta},\underline{d\mathfrak{s}}) = \mathrm{tr}_\Sigma \underline{du}$, where

$$\frac{1}{c^2}\underline{du}_{tt} - \triangle \underline{du} + \tilde{D}\underline{du} = -\big(\underline{d\mathfrak{s}}(x)\, u - \underline{d\eta}(x)\, u^2\big)_{tt} \quad \text{in } \Omega \times (0,T)$$

Using two well-chosen excitations $\tilde{r}_1$, $\tilde{r}_2$, from Theorem 2.1 we have linearised injectivity of the two component forward operator $\vec{F} = (F_1, F_2)$ with $F_i = C \circ S_i$ and $S_i : (\eta,\mathfrak{s}) \mapsto u_i$ defined as the parameter-to-state map for (5) with $\tilde{r} = \tilde{r}_i$, $i \in \{1,2\}$. Thus we conclude formal well-definedness of a frozen Newton scheme by

$$(\eta_{n+1},\mathfrak{s}_{n+1}) = (\eta_n,\mathfrak{s}_n) + (\underline{d\eta},\underline{d\mathfrak{s}}) \text{ where } (\underline{d\eta},\underline{d\mathfrak{s}}) \text{ solves } \vec{F}'(\eta_0,\mathfrak{s}_0)(\underline{d\eta},\underline{d\mathfrak{s}}) = \vec{h} - \vec{F}(\eta_n,\mathfrak{s}_n)$$

provided that $\vec{h} - \vec{F}(\eta_n,\mathfrak{s}_n)$ lies in the range of $\vec{F}'(\eta_0,\mathfrak{s}_0)$. However, the inverse problem inherits the ill-posedness from the original nonlinear one and the given data is typically contaminated with noise, that is, in place of $\vec{h} = (h_1,h_2)$ we only have $\vec{h}^\delta \approx \vec{h}$. Thus regularisation needs to be applied and the convergence analysis of the resulting iterative reconstruction scheme requires structural conditions on the forward operator. One of the conditions allowing for convergence guarantees is range invariance of the linearised forward operator (as plausible from the above requirement of the residual lying in the range of $\vec{F}'(\eta_0,\mathfrak{s}_0)$) and can be established for our problem in the slightly relaxed form

$$\vec{F}(\eta,\vec{\mathfrak{s}}) - \vec{F}(\eta_0,\vec{\mathfrak{s}}_0) = \vec{F}'(\eta_0,\vec{\mathfrak{s}}_0)(\underline{d\eta}(\eta,\vec{\mathfrak{s}}),\underline{\vec{d\mathfrak{s}}}(\eta,\vec{\mathfrak{s}})). \tag{20}$$

To illustrate this first of all in the single excitation case

$$F(\eta,\mathfrak{s}) - F(\eta_0,\mathfrak{s}_0) = F'(\eta_0,\mathfrak{s}_0)(\underline{d\eta}(\eta,\mathfrak{s}),\underline{d\mathfrak{s}}(\eta,\mathfrak{s})), \tag{21}$$

note that it is straightforward to see that by setting

$$\begin{aligned}
&\underline{d\eta}(\eta,\mathfrak{s}) = \underline{d\eta}(\eta) := \eta - \eta_0,\\
&\underline{d\mathfrak{s}}(\eta,\mathfrak{s}) = \underline{d\mathfrak{s}}(\eta,\mathfrak{s};u,u_0) := \frac{1}{u_0}\Big((\mathfrak{s}-\mathfrak{s}_0)u - (\eta-\eta_0)(u^2-u_0^2) - \eta_0(u-u_0)^2\Big)
\end{aligned} \tag{22}$$

we can satisfy the identity (21). However, through time dependence of u_0 and u, the expression for $\underline{d\mathfrak{s}}(\eta,\mathfrak{s})$ in the second identity of (22) will be time dependent as well. Thus we consider $\mathfrak{s}$ as a space *and* time dependent function. Moreover, we have to take into account two excitations resulting in two different states u^i, $i \in \{1,2\}$ and thus also need two copies of $\mathfrak{s}$ to be able to capture this in (22), thus considering $\vec{\mathfrak{s}}(x,t) = (\mathfrak{s}^1(x,t),\mathfrak{s}^2(x,t))$. Introducing so much additional dimensionality in parameter space clearly counteracts uniqueness and after all our aim is to reconstruct only one only space dependent $\mathfrak{s}(x)$ (along with the nonlinearity coefficient $\eta(x)$). This is achieved by penalisation with an operator

$$P : (\mathfrak{s}^1,\mathfrak{s}^2) \mapsto (\mathfrak{s}^1 - \mathrm{Proj}_{\mathrm{const}}^{L^2(0,T;\mu)}\mathfrak{s}^1, \mathfrak{s}^2 - \mathrm{Proj}_{\mathrm{const}}^{L^2(0,T;\mu)}\mathfrak{s}^2) \tag{23}$$

where $\mathrm{Proj}_{\mathrm{const}}^{L^2_\mu(0,T)}$ is the L^2_μ projection on the space of constant functions with a finite measure μ on $(0,T)$, including the case of an infinite time horizon $T=\infty$. Note that in the latter case we do not use μ as the ordinary Lebesgue measure λ, since this would exclude the constant-in-time solutions that we are actually looking for but, e.g., define μ by $d\mu(t) = t^{-2}d\lambda(t)$.
Setting $(\eta_0,\vec{\mathfrak{s}}_0) = (0,1/c^2,1/c^2)$ and abbreviating

$$\begin{aligned}
&K := \vec{F}'(\eta_0,\vec{\mathfrak{s}}_0), \quad \vec{h}_0 = \vec{h} - \vec{F}(\eta_0,\vec{\mathfrak{s}}_0),\\
&r : (\eta,\mathfrak{s}^1,\mathfrak{s}^2) \mapsto (\underline{d\eta}(\eta), \underline{d\mathfrak{s}}(\eta,\mathfrak{s}^1;u^1,u_0^1), \underline{d\mathfrak{s}}(\eta,\mathfrak{s}^2;u^2,u_0^2)) \text{ as in (22)},
\end{aligned}$$

we can thus write the original inverse problem (7) equivalently as a combination of an ill-posed linear and a well-posed nonlinear problem

$$\begin{aligned}
&K\hat{r} = \vec{h}_0\\
&r(\eta,\vec{\mathfrak{s}}) = \hat{r}\\
&P\vec{\mathfrak{s}} = 0
\end{aligned} \tag{24}$$

for the unknowns $(\eta,\vec{\mathfrak{s}},\hat{r})$. In view of (22) we expect r to be close to the identity in the sense of

$$\exists\, c_r \in (0,1)\, \forall (\eta,\vec{\mathfrak{s}}) \in U(\subseteq X) \,:\, \|(\underline{d\eta}(\eta,\vec{\mathfrak{s}}), \underline{\vec{d\mathfrak{s}}}(\eta,\vec{\mathfrak{s}})) - (\eta-\eta_0,\vec{\mathfrak{s}}-\vec{\mathfrak{s}}_0)\|_X \le c_r \|(\eta-\eta_0,\vec{\mathfrak{s}}-\vec{\mathfrak{s}}_0)\|_X \tag{25}$$

for some sufficiently small neighborhood $U \subseteq X$ of the exact solution $(\eta^\dagger,\vec{\mathfrak{s}}^\dagger)$, an estimate that we will establish in an appropriate function space setting X in the proof of Theorem 3.1 below. The symbol $\vec{\mathfrak{s}}^\dagger$ is hard to identify and given previous nightmares with IP typsetting out of latex .....

Thus, a natural way of making use of the structure (24) in a regularised frozen Newton type method is to define iterates for $\vec{x} = (\eta, \mathfrak{s}^1, \mathfrak{s}^2)$ with $r(x) \approx x - x_0$ as minimizers of

$$x^\delta_{n+1} \in \operatorname{argmin}_{x \in \mathcal{D}(\vec{F})} \|K(x - x^\delta_n) + \vec{F}(x^\delta_n) - h^\delta\|_Y^p + \alpha_n \mathcal{R}(x) + \|Px\|_Z^2. \tag{26}$$

with a proper X lower semicontinuous functional $\mathcal{R}$, a sequence of positive regularisation parameters tending to zero $(\alpha_n)_{n\in\mathbb{N}} \subseteq \mathbb{R}^+$, $\alpha_n \overset{n\to\infty}{\longrightarrow} 0$ and P as in (23), $Z := L^2_\mu(0,T;L^2(\Omega))^2$. In view of the well-posedness results quoted above, we choose $X \subseteq L^\infty(\Omega) \times L^\infty(0,T;L^\infty(\Omega))^2$ and $Y \supseteq L^\infty(0,T;L^\infty_\nu(\Sigma))$ with ν being just the Lebesgue measure in case of a smooth manifold Σ and the counting measure in case σ consists of discrete points.

This includes the Hilbert space setting

$$\begin{aligned} &X = X_\eta \times X^2_{\mathfrak{s}} \text{ with } X_\eta = H^\sigma(\Omega),\ X_{\mathfrak{s}} = H^\tau(0,T;H^1(\Omega)) \cap L^2(0,T;H^2(\Omega)),\\ &Y = L^2(0,T;L^2_\nu(\Sigma))^2 \end{aligned} \tag{27}$$

in space dimensions $d \in \{1,2,3\}$ for any $\sigma > d/2$, $\tau > 1/2$, since due to Sobolev's and Agmon's interpolation inequality [4], $X_{\mathfrak{s}}$ continuously embeds into $L^\infty(\Omega)\times L^\infty(0,T;L^\infty(\Omega))$. With this and $\mathcal{R}(x) = \|x - x_0\|_X^2$ we can write (26) as

$$\vec{x}^\delta_{n+1} = \vec{x}^\delta_n + (K^\star K + P^\star P + \alpha_n I)^{-1}\Big(K^\star(\vec{h}^\delta - \vec{F}(\vec{x}^\delta_n)) - P^\star P\vec{x}^\delta_n + \alpha_n(\vec{x}_0 - \vec{x}^\delta_n)\Big) \tag{28}$$

where $K^\star$ denotes the Hilbert space adjoint of $K : X \to Y$.

In case of noisy data with noise level δ satisfying the bound

$$\|\vec{h}^\delta - \vec{F}(\eta^\dagger, \mathfrak{s}^\dagger)\|_{L^2(0,T;L^2(\Omega))} \le \delta \tag{29}$$

we have to stop the iteration according to

$$n_*(\delta) \to 0, \quad \delta \sum_{j=0}^{n_*(\delta)-1} c_r^j \alpha^{-1/2}_{n_*(\delta)-j-1} \to 0 \qquad \text{as } \delta \to 0 \tag{30}$$

with c_r as in (25). With the simple geometric sequence $\alpha_n = \alpha_0\theta^n$ for some $\theta \in (0,1)$, this just corresponds to the usual a priori choice $\alpha_{n_*(\delta)} \to 0$ and $\delta^2/\alpha_{n_*(\delta)-1}$.

From [22, Theorem 2.2] and Theorem 2.1 we thus conclude the following convergence result.

Theorem 3.1 *Let the conditions of Theorem 2.1 on the observation set Σ and on the excitations $\tilde{r}^1$, $\tilde{r}^2$ be satisfied. Let $\vec{x}_0 = (\eta_0, \mathfrak{s}^1_0, \mathfrak{s}^2_0) \in U := \mathcal{B}_\rho(\vec{x}^\dagger)$ for some $\rho > 0$ sufficiently small, assume that $u^i_0 = S^i(\eta_0, \mathfrak{s}^1_0, \mathfrak{s}^2_0)$ is bounded away from zero*

$$|u^i_0| \ge \underline{c} > 0 \quad \text{a.e. on } (0,T)\times\Omega,\ i \in \{1,2\}, \tag{31}$$

and let the stopping index $n_* = n_*(\delta)$ be chosen according to (30).

Then the iterates $(\vec{x}^\delta_n)_{n\in\{1,\dots,n_*(\delta)\}}$ are well-defined by (28)*, remain in $\mathcal{B}_\rho(\vec{x}^\dagger)$ and converge in X (defined as in* (27) *with $\tau \in (1,5/4)$), $\|\vec{x}^\delta_{n_*(\delta)} - \vec{x}^\dagger\|_X \to 0$ as $\delta \to 0$. In the noise free case $\delta = 0$, $n_*(\delta) = \infty$ we have $\|\vec{x}_n - \vec{x}^\dagger\|_X \to 0$ as $n \to \infty$.*

[4] $\|v\|^2_{L^\infty(\Omega)} \le C\|v\|_{H^1(\Omega)}\|v\|_{H^2(\Omega)}$

Maybe remark here that we will comment on the assumption (31) shortly?

Proof. With $\tau \in (1, 5/4)$, the solution space V defined in (19) is embedded in $H^\tau(0,T;L^\infty(\Omega)\cap W^{1,3}(\Omega))$ and on the other hand the parameter space $X_{\mathfrak{s}}$ defined in (27) is embedded in $L^\infty(0,T;L^\infty(\Omega)) \cap H^\tau(0,T;L^6(\Omega))$; moreover $\eta - \eta_0$ and η_0 are time-independent. Using the fact that $H^\tau(0,T)$ and $H^2(\Omega)$ are Banach algebras, we obtain the following estimates. We start from the identity

$$\underline{d\mathfrak{s}}(\eta,\mathfrak{s}) - (\mathfrak{s}-\mathfrak{s}_0) = \tfrac{1}{u_0}(u-u_0)\Big((\mathfrak{s}-\mathfrak{s}_0) - (\eta-\eta_0)(u+u_0) - \eta_0(u-u_0)\Big),$$

and, using the above mentioned continuous embeddings, estimate the individual terms as follows

$$\begin{aligned}
\|\tfrac{1}{u_0}(u-u_0)(\mathfrak{s}-\mathfrak{s}_0)\|_{L^2(H^2)} &\le \|\tfrac{1}{u_0}\|_{L^\infty(H^2)}\|u-u_0\|_{L^\infty(H^2)}\|\mathfrak{s}-\mathfrak{s}_0\|_{L^2(H^2)}\\
\|\tfrac{1}{u_0}(u-u_0)(\mathfrak{s}-\mathfrak{s}_0)\|_{H^\tau(H^1)} &\le \|\tfrac{1}{u_0}\|_{H^\tau(L^\infty)}\|u-u_0\|_{H^\tau(L^\infty)}\|\mathfrak{s}-\mathfrak{s}_0\|_{H^\tau(H^1)}\\
&\quad + \Big(\|\tfrac{1}{u_0}\|_{H^\tau(L^\infty)}\|(u-u_0)\|_{H^\tau(W^{1,3})} + \|\tfrac{1}{u_0}\|_{H^\tau(W^{1,3})}\|u-u_0\|_{H^\tau(L^\infty)}\Big)\|\mathfrak{s}-\mathfrak{s}_0\|_{H^\tau(L^6)}
\end{aligned}$$

$$\begin{aligned}
\|\tfrac{1}{u_0}(u-u_0)(u+u_0)(\eta-\eta_0)\|_{L^2(H^2)} &\le \|\tfrac{1}{u_0}\|_{L^2(H^2)}\|u-u_0\|_{L^\infty(H^2)}\|u+u_0\|_{L^\infty(H^2)}\|\eta-\eta_0\|_{H^2}\\
\|\tfrac{1}{u_0}(u-u_0)(u+u_0)(\eta-\eta_0)\|_{H^\tau(H^1)} &\le \|\tfrac{1}{u_0}\|_{H^\tau(L^\infty)}\|u-u_0\|_{H^\tau(L^\infty)}\|u+u_0\|_{H^\tau(L^\infty)}\|\eta-\eta_0\|_{H^1}\\
&\quad + \Big(\|\tfrac{1}{u_0}\|_{H^\tau(L^\infty)}\|u-u_0\|_{H^\tau(L^\infty)}\|(u+u_0)\|_{H^\tau(W^{1,3})}\\
&\qquad + \|\tfrac{1}{u_0}\|_{H^\tau(L^\infty)}\|u-u_0\|_{H^\tau(W^{1,3})}\|(u+u_0)\|_{H^\tau(L^\infty)}\\
&\qquad + \|\tfrac{1}{u_0}\|_{H^\tau(W^{1,3})}\|u-u_0\|_{H^\tau(L^\infty)}\|(u+u_0)\|_{H^\tau(L^\infty)}\Big)\|\eta-\eta_0\|_{H^\tau(L^6)}
\end{aligned}$$

and analogously for the term $\frac{1}{u_0}(u-u_0)^2\eta_0$.
This together with assumption (31) and Lipschitz continuity of S allow us to establish a bound of the form

$$\|(\underline{d\eta}(\eta,\vec{\mathfrak{s}}),\underline{\vec{d\mathfrak{s}}}(\eta,\vec{\mathfrak{s}})) - (\eta-\eta_0,\vec{\mathfrak{s}}-\vec{\mathfrak{s}}_0)\|_X \le C\|(\eta-\eta_0,\vec{\mathfrak{s}}-\vec{\mathfrak{s}}_0)\|_X^2$$

which in a sufficiently small neighborhood of $(\eta_0,\vec{\mathfrak{s}}_0)$ yields the estimate (25) with small c_r.

♢

3.1.1 An all-at-once formulation

As can be seen from the proof of Theorem 3.1, we need to avoid division by zero by assuming (31); however, as a solution to a wave equation, u_0 will typically change sign. This problem can be circumvented by considering the all-at-once version, which allows us to choose u_0 not necessarily as a PDE solution and also allows for much more freedom in the choice of the function spaces.

To this end, we consider the model and the observation equation as a system of operator equations for the sought-after coefficients and the states. That is, we set $\vec{x} = (\eta, \mathfrak{s}^1, \mathfrak{s}^2, u^1, u^2)$ and replace the definition of $\vec{F} = (F_1, F_2)$ by

$$F_i(\eta, \mathfrak{s}^1, \mathfrak{s}^2, u^1, u^2) = \begin{pmatrix} F^{\mathrm{mod}}(\eta, \mathfrak{s}^i, u^i) \\ \mathrm{tr}_\Sigma u^i \end{pmatrix}$$

where

$$\begin{aligned} \langle F^{\mathrm{mod}}(\eta, \mathfrak{s}, u), w\rangle_{W^*,W} &= \int_0^T \int_\Omega \Big(\big(\mathfrak{s}(x)u - \eta(x)u^2\big)\, w_{tt} + (-\triangle u + \tilde{D}u)\, w \Big)\, dx\, dt \\ w \in W &:= \{v \in H^2(0,T;L^2(\Omega)) \ : \ v(T) = 0,\ v_t(T) = 0\}, \end{aligned} \tag{32}$$

where $\langle \cdot, \cdot \rangle_{W^*,W}$ denotes the dual pairing in W.[5] Note that we aim here to allow for low regularity of the coefficients to decrease the degree of ill-posedness of the inverse problem as much as possible. This is enabled by the weak formulation (with respect to time derivatives) of the PDE model in (32) and allows to use the function spaces

$$\begin{aligned} &X = X_\eta \times X_\mathfrak{s}^2 \times X_u^2 \text{ with } X_\eta = L^2(\Omega),\ X_\mathfrak{s} = L^2(0,T;L^2(\Omega)), \\ &X_u = \begin{cases} L^2(0,T;H^2(\Omega)) \cap H^{\tilde{\alpha}}(0,T;\dot{H}^{\tilde{\beta}}(\Omega)) \text{ in case of CH} \\ H^{\tilde{\alpha}_1}(0,T;H^2(\Omega)) \cap H^{\tilde{\alpha}_1+2}(0,T;L^2(\Omega)) \text{ in case of FZ} \end{cases} \\ &Y = (W^*)^2 \times L^2(0,T;L^2_\nu(\Sigma))^2. \end{aligned} \tag{33}$$

Here the exponents are chosen such that $\tilde{D}$ maps X_u into $L^2(0,T;L^2(\Omega))$ and X_u continuously embeds into $L^\infty(0,T;L^\infty(\Omega))$:

$$\tilde{\alpha} \geq \alpha,\ \tilde{\beta} \geq \beta,\ \tilde{\alpha}_1 \geq \alpha_1,\ \tilde{\alpha}_2 \geq \alpha_2,\ \tilde{\alpha} > \frac{1}{2},\ \tilde{\beta} > \frac{d}{2},\ \max\{\tilde{\alpha}_1, \tilde{\alpha}_2\} > 0\,. \tag{34}$$

The range invariance condition

$$\vec{F}(\eta, \vec{\mathfrak{s}}, \vec{u}) - \vec{F}(\eta_0, \vec{\mathfrak{s}}_0, \vec{u}_0) = \vec{F}'(\eta_0, \vec{\mathfrak{s}}_0, \vec{u}_0)(\underline{d\eta}(\eta, \vec{\mathfrak{s}}), \underline{\vec{d\mathfrak{s}}}(\eta, \vec{\mathfrak{s}})\underline{\vec{du}}(\eta, \vec{\mathfrak{s}}))$$

can be verified with $\underline{d\eta}$, $\underline{d\mathfrak{s}}$ defined as in (22) and $\underline{du} = u - u_0$. Injectivity of $\vec{F}'(0, 1/c^2, 1/c^2, u_0^1, u_0^2)$ can be shown analogously to Theorem 2.1, for $u_i^0(x,t) = \phi(x)\psi_i(t)$ with $\phi \in \mathcal{D}(-\triangle)$, $\phi \neq 0$ a.e. in Ω, ψ_1, ψ_2 satisfying (16), but actually without u_i^0 needing to solve (5). Finally, the estimate of $r(\vec{x}) - (\vec{x} - \vec{x}_0)$ simplifies to

$$\begin{aligned} \|r(\vec{x}) - (\vec{x} - \vec{x}_0)\|_X^2 &== \sum_{i=1}^2 \|\tfrac{1}{u_0}(u - u_0)\Big((\mathfrak{s} - \mathfrak{s}_0) - (\eta - \eta_0)(u + u_0) - \eta_0(u - u_0) \Big)\|^2_{L^2(L^2)} \\ \leq \sum_{i=1}^2 \|\tfrac{1}{u_0}\|^2_{L^\infty(L^\infty)} &\|(u - u_0)\|^2_{L^\infty(L^\infty)} \Big(\|\mathfrak{s} - \mathfrak{s}_0\|_{L^2} \\ &+ \|\eta - \eta_0\|_{L^2(L^2)}\|u + u_0\|_{L^\infty(L^\infty)} + \|\eta_0\|_{L^2(L^2)}\|u - u_0\|_{L^\infty(L^\infty)} \Big)^2. \end{aligned}$$

[5] for $T = \infty$ the end conditions are to be understood in a limiting sense $\lim_{t\to\infty} v(t) = 0$, $\lim_{t\to\infty} v_t(t) = 0$

Thus, applicability and convergence of the frozen Newton method transfers to this all-at-once setting as follows.

Theorem 3.2 *Let the conditions of Theorem 2.1 on the observation set Σ and on the functions ϕ, ψ_1, ψ_2 in $u_i^0(x,t) = \phi(x)\psi_i(t)$ be satisfied. Let $\vec{x}_0 = (\eta_0, \mathfrak{s}_0^1, \mathfrak{s}_0^2, u_0^1, u_0^2) \in U := \mathcal{B}_\rho(\vec{x}^\dagger)$ for some $\rho > 0$ sufficiently small, and let the stopping index $n_* = n_*(\delta)$ be chosen according to* (30).

Then the iterates $(\vec{x}_n^\delta)_{n\in\{1,\dots,n_*(\delta)\}}$ are well-defined by (28)*, remain in $\mathcal{B}_\rho(\vec{x}^\dagger)$ and converge in X (defined as in* (33) *with* (34)*), $\|\vec{x}_{n_*(\delta)}^\delta - \vec{x}^\dagger\|_X \to 0$ as $\delta \to 0$. In the noise-free case $\delta = 0$, $n_*(\delta) = \infty$ we have $\|\vec{x}_n - \vec{x}^\dagger\|_X \to 0$ as $n \to \infty$.*

The price to pay for this more relaxed setting is convergence of the coefficients in a weaker norm as compared to Theorem 3.1.

3.2 Reconstructions

In this section we show reconstructions of $\eta(x)$, $\mathfrak{s}(x)$ in (5) with Caputo-Wismer-Kelvin damping, that is,

$$\begin{aligned} \big(\mathfrak{s}(x)u - \eta(x)u^2\big)_{tt} - \triangle u - b\triangle\partial_t^\alpha u = \tilde{r} \quad \text{in } \Omega\times(0,T) \\ \partial_\nu u + \gamma u = 0 \text{ on } \partial\Omega\times(0,T), \quad u(0) = 0, \quad u_t(0) = 0 \quad \text{in } \Omega. \end{aligned} \tag{35}$$

in one space dimension $\Omega = (0,1)$ with Dirichlet-Neumann conditions $\gamma(0) = \infty$, $\gamma(1) = 0$ from measurements at two points $\Sigma = (0.1, 1)$. (Note that since we impose homogeneous Dirichlet boundary conditions at the left endpoint, measuring u there would not provide any additional information; indeed, also in practice the transducer array will be immersed into the overall computational domain Ω.)

For the numerical solution of (35), we follow the method of [25] and rewrite the equation by integrating once with respect to time

$$\begin{aligned} \big(\mathfrak{s}(x) - 2\eta(x)u\big)u_t - \tilde{b}\triangle I_t^{1-\alpha}u - \triangle I_t^1 u = I_t^1\tilde{r} \quad \text{in } \Omega\times(0,T) \\ \partial_\nu u + \gamma u = 0 \text{ on } \partial\Omega\times(0,T), \quad u(0) = 0 \quad \text{in } \Omega, \end{aligned} \tag{36}$$

to which we apply a modified Crank-Nicolson solver taking into account the fractional integral term. Likewise for its linearisation (10).

To test the frozen Newton method from Section 3.1, we consider three scenarios A, B and C as described below. While the theory from Section 3.1 requires two executions[6] and an extension of $\mathfrak{s}$ to a time dependent function, this was not needed in practical computations. The reconstructions shown here are based on a single excitation, but carrying out measurements at two points $\Sigma = \{0.1, 1\}$. Also $\mathfrak{s}$ is treated as a function of x only. Both

[6] maybe use "experiments" or "excitatons" rather than "executions"?

coefficients were discretised using a chapeau basis set and the starting values were $\eta_0 = 0$ and $\mathfrak{s} = 1$.

Figures 1 and 2 show a simultaneous reconstruction of both $\eta(x)$ and $\mathfrak{s}(x)$ under 1% and 0.1% noise in the time trace data. Here the value of the solution $u(x,t)$ was negative and there was therefore no cancellation effect on the $\mathfrak{s}(x)$ and the $\eta(x)$ term (test case A). In

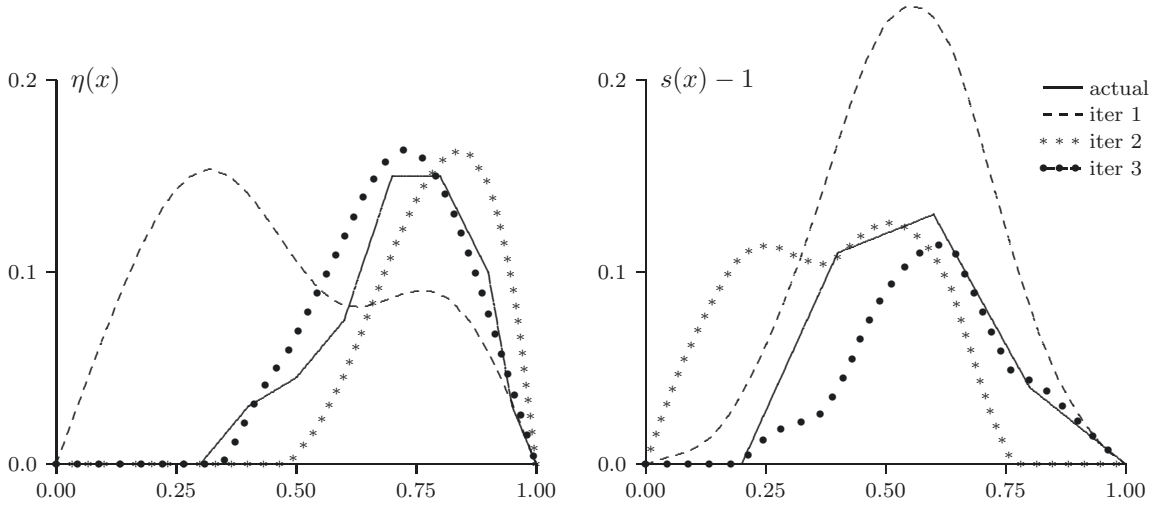

Figure 1: **Reconstruction of both $\eta(x)$ and $\mathfrak{s}(x)$ under 1% data noise; test case A.**

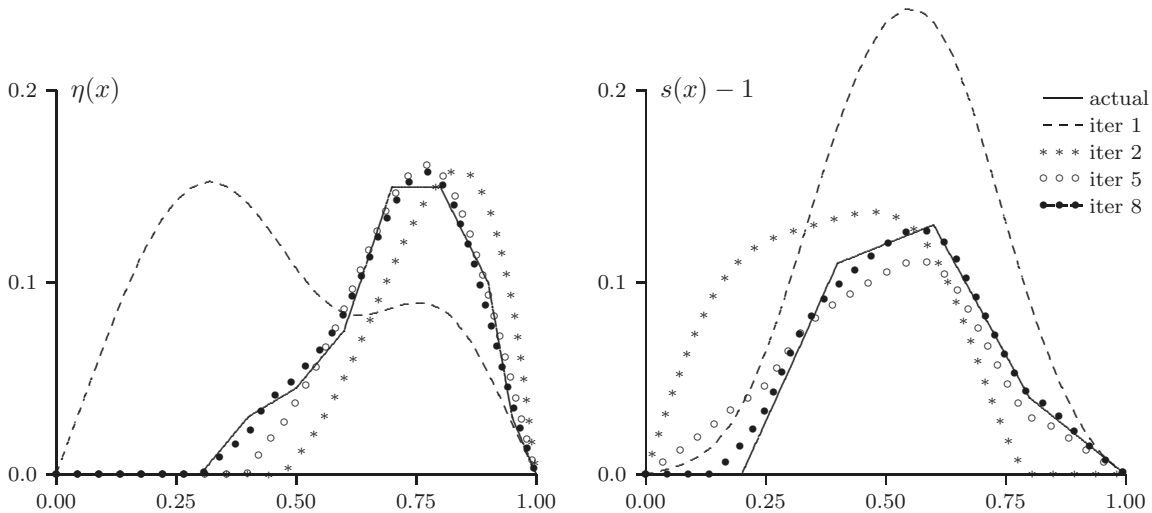

Figure 2: **Reconstruction of both $\eta(x)$ and $\mathfrak{s}(x)$ under 0.1% data noise; test case A.**

Figure 3 we show the difference when the sign of $u(x,t)$ is reversed so that there is the potential for a cancellation effect between $\eta(x)$ and $\mathfrak{s}(x)$ (test case B). In fact this occurred resulting in a poorer reconstruction in both functions. Data noise here was again 0.1%. The final picture 4 shows a more complex function $\eta(x)$ with two features (test case C), one at each end of the interval. For this run the function $u(x,t)$ was zero at the endpoint

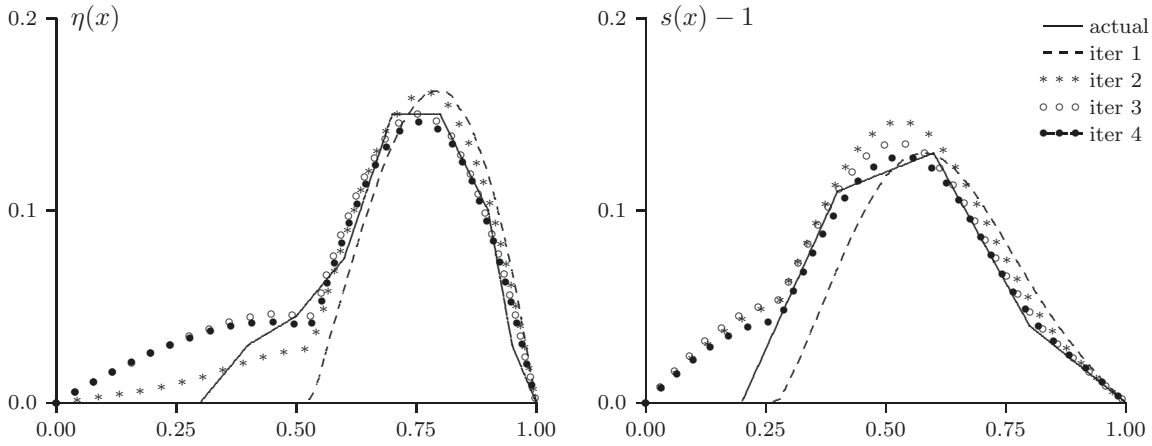

Figure 3: **Reconstruction of both $\eta(x)$ and $\mathfrak{s}(x)$ under 0.1% data noise; test case B.**

$x = 0$ and so small in comparison at the left end as opposed to the right. Since η occurs in combination with u in the equation this means a relative loss of information at the left-hand endpoint. This is clearly visible from the left hand graphic. In, addition this error in $\eta(x)$ now affects the combined term $(\mathfrak{s} - \eta u)$ and results in a similarly poor reconstruction of $\mathfrak{s}(x)$ near $x = 0$. Note that a seemingly overall better match of η at the fourth iterate is dismissed in subsequent iterations that are much worse in approximating the left hand feature. [7] This is due to the fact that the mismatch is weighed by the values of u which are small near the left endpoint, but penalize deviations occurring in the right half of the interval (as is the case for iteration 4) much more strongly. These reconstructions were made using 0.1% data noise.

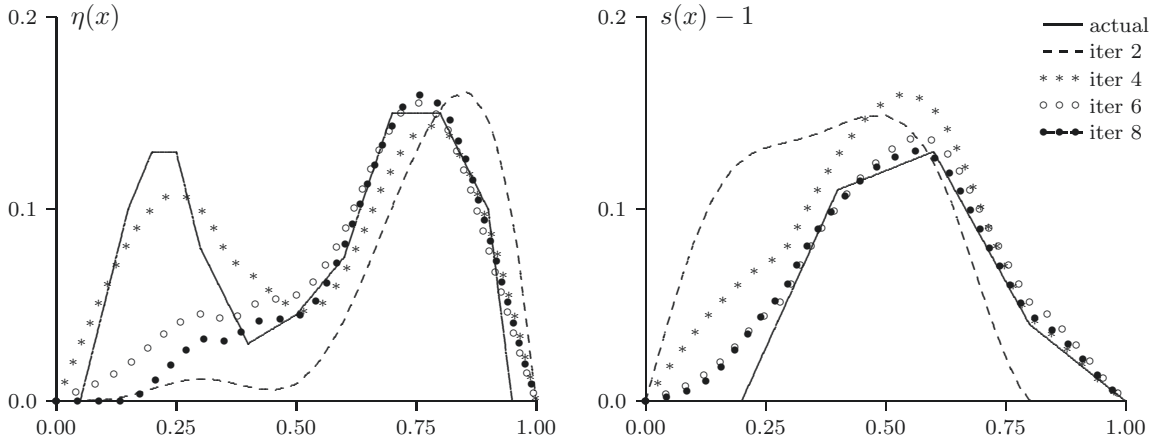

Figure 4: **Reconstruction of both $\eta(x)$ and $\mathfrak{s}(x)$ under 0.1% data noise; test case C.**

This effect of smallness of u at the left hand endpoint is also apparent in the other figures, particularly in the case where there is a significant feature near this endpoint. In all figures

[7] textcolorredShould we add further comment here on this? Such as stopping condition?]not sure how ...]

we imposed the sign constraint imposed by the physical problem that $\eta(x) \geq 0$.

For an η function with support away from $x = 0$ the reconstructions shown in figure 2 under 0.1% noise and in figure 1 with 1% added noise indicate a reasonable reconstruction of both η and $\mathfrak{s}(x)$. Note that a poor initial guess (both these functions taken to be constant zero and one respectively) leads to a severe overshoot in the first computed approximation to $\mathfrak{s}(x)$ although this quickly settles down. In this case both actual $\mathfrak{s}(x)$ and $\eta(x)$ functions have support away from the left-hand endpoint $x = 0$ and there is also overshoot in the first iteration of η.

The difference between (0.1%) and 1% of added noise to the data simulated by the direct solver is quite apparent and indicates the severe ill-conditioning of the inverse problem.

Finally, we show a plot of the singular values of the Jacobian matrix frozen at $\mathfrak{s}(x) = 1$ and $\eta(x) = 0$. As Figure 5 shows there is indeed an exponential decay of the singular values and the initial steep decay of the largest values means that under even relatively small noise in the data it will be difficult to use more than about ten relevant modes as the above reconstruction figures demonstrate. However the decay rate of the singular values overall is actually more favourable for reconstructions than for classical exponentially ill-posed problems such as the backwards or sideways heat problems, the Cauchy problem for the Laplacian or inverse obstacle scattering.

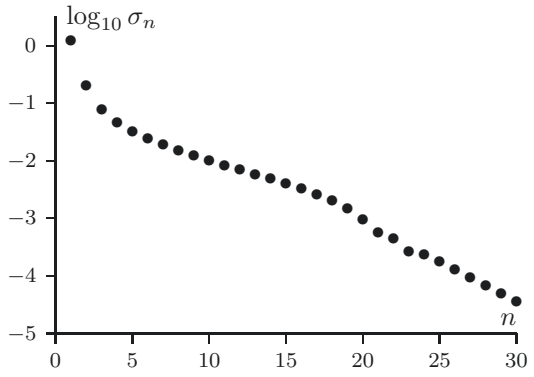

Figure 5: **Singular values of the Jacobian.**

All of the above reconstructions were obtained using the value $\alpha = \frac{1}{2}$ but none were sensitive to this parameter except for the extreme ends of its range. However, it is certainly the situation if we had $\alpha = 1$ and thus exponential damping the usefulness of the resulting very small values of u obtained from anything beyond modest time values would be extremely limited – in particular for the reconstruction of $\eta(x)$ as this is inherently coupled to the magnitude of u. [8]

Two-dimensional reconstructions in the practically relevant case of a piecewise constant coefficient η, corresponding to inclusions in a homogeneous background, can be found in [27].

Acknowledgment

The work of the second author was supported in part by the National Science Foundation through award DMS -2111020.

[8] Is it worth making any sort of remark about likely effects of having $(\triangle)^{\beta}$?

References

[1] Sebastian Acosta, Gunther Uhlmann, and Jian Zhai. Nonlinear ultrasound imaging modeled by a Westervelt equation. *SIAM Journal on Applied Mathematics*, 82(2):408–426, 2022.

[2] Melody Alsaker, Diego A C Cárdenas, Sergio S Furuie, and Jennifer L Mueller. Complementary use of priors for pulmonary imaging with electrical impedance and ultrasound computed tomography. *J Comput Appl Math*, 395:113591, 2021.

[3] Arash Anvari, Flemming Forsberg, and Anthony E. Samir. A primer on the physical principles of tissue harmonic imaging. *RadioGraphics*, 35(7):1955–1964, 2015. PMID: 26562232.

[4] Alain Bamberger, Roland Glowinski, and Quang Huy Tran. A domain decomposition method for the acoustic wave equation with discontinuous coefficients and grid change. *SIAM J.NUMER.ANAL.*, 34(2):603–639, April 1997.

[5] L. Bjørnø. Characterization of biological media by means of their non-linearity. *Ultrasonics*, 24(5):254 – 259, 1986.

[6] V. Burov, I. Gurinovich, O. Rudenko, and E. Tagunov. Reconstruction of the spatial distribution of the nonlinearity parameter and sound velocity in acoustic nonlinear tomography. *Acoustical Physics*, 40:816–823, 11 1994.

[7] Wei Cai, Wen Chen, Jun Fang, and Sverre Holm. A Survey on Fractional Derivative Modeling of Power-Law Frequency-Dependent Viscous Dissipative and Scattering Attenuation in Acoustic Wave Propagation. *Applied Mechanics Reviews*, 70(3), 2018.

[8] Charles A. Cain. Ultrasonic reflection mode imaging of the nonlinear parameter b/a: I. a theoretical basis. *The Journal of the Acoustical Society of America*, 80(1):28–32, 1986.

[9] Michele Caputo. Linear models of dissipation whose q is almost frequency independent-ii. *Geophysical Journal of the Royal Astronomical Society*, 13(5):529–539, 1967.

[10] W. Chen and S. Holm. Fractional laplacian time-space models for linear and nonlinear lossy media exhibiting arbitrary frequency power-law dependency. *The Journal of the Acoustical Society of America*, 115(4):1424–1430, 2004.

[11] Mostafa Fatemi and James F Greenleaf. Ultrasound-stimulated vibro-acoustic spectrography. *Science*, 280:82–85, 1998.

[12] Mostafa Fatemi and James F. Greenleaf. Vibro-acoustography: An imaging modality based on ultrasound-stimulated acoustic emission. *Proceedings of the National Academy of Sciences*, 96(12):6603–6608, 1999.

[13] Hartmut Gemmeke, Torsten Hopp, Michael Zapf, Clemens Kaiser, and Nicole V. Ruiter. 3d ultrasound computer tomography: Hardware setup, reconstruction methods and first clinical results. *Nuclear Instruments and Methods in Physics Research Section A: Accelerators, Spectrometers, Detectors and Associated Equipment*, 873:59–65, 2017. Imaging 2016.

[14] James F. Greenleaf, S. A. Johnson, S. L. Lee, G. T. Hermant, and E. H. Woo. Algebraic reconstruction of spatial distributions of acoustic absorption within tissue from their two-dimensional acoustic projections. In Philip S. Green, editor, *Acoustical Holography: Volume 5*, pages 591–603. Springer US, Boston, MA, 1974.

[15] Mark F. Hamilton and David T. Blackstock. *Nonlinear Acoustics*. Academic Press, New York, 1997.

[16] Sverre Holm and Sven Peter Näsholm. A causal and fractional all-frequency wave equation for lossy media. *The Journal of the Acoustical Society of America*, 130(4):2195–2202, 2011.

[17] Nobuyuki Ichida, Takuso Sato, and Melvin Linzer. Imaging the nonlinear ultrasonic parameter of a medium. *Ultrasonic Imaging*, 5(4):295–299, 1983. PMID: 6686896.

[18] Ashkan Javaherian, Felix Lucka, and Ben T. Cox. Refraction-corrected ray-based inversion for three-dimensional ultrasound tomography of the breast. *Inverse Problems*, 36(12):125010, 41, 2020.

[19] B. Kaltenbacher and I. Lasiecka. Global existence and exponential decay rates for the Westervelt equation. *Discrete and Continuous Dynamical Systems (DCDS)*, 2:503–525, 2009.

[20] Barbara Kaltenbacher. Mathematics of Nonlinear Acoustics. *Evolution Equations and Control Theory (EECT)*, 4:447–491, 2015. open access: https://www.aimsciences.org/article/doi/10.3934/eect.2015.4.447.

[21] Barbara Kaltenbacher. Periodic solutions and multiharmonic expansions for the Westervelt equation. *Evolution Equations and Control Theory EECT*, 10:229–247, 2021.

[22] Barbara Kaltenbacher. Convergence guarantees for coefficient reconstruction in PDEs from boundary measurements by variational and Newton type methods via range invariance. 2022. submitted and arXiv:2209.12596 [math.NA].

[23] Barbara Kaltenbacher. On the inverse problem of vibro-acoustography. *Meccanica*, 2022. to appear; https://doi.org/10.1007/s11012-022-01485-w; see also arXiv:2109.01907 [math.AP].

[24] Barbara Kaltenbacher and William Rundell. On the identification of the nonlinearity parameter in the Westervelt equation from boundary measurements. *Inverse Problems & Imaging*, 15:865–891, 2021.

[25] Barbara Kaltenbacher and William Rundell. On an inverse problem of nonlinear imaging with fractional damping. *Mathematics of Computation*, 91:245–276, 2022. see also arXiv:2103.08965 [math.AP].

[26] Barbara Kaltenbacher and William Rundell. *Inverse Problems for Fractional Partial Differential Equations*. Graduate Studies in Mathematics. AMS, 2023. to appear.

[27] Barbara Kaltenbacher and William Rundell. Nonlinearity parameter imaging in the frequency domain. 2023. submitted; see also arXiv:2303.09796 [math.NA].

[28] Felix Lucka, Mailyn Pérez-Liva, Bradley E. Treeby, and Ben T. Cox. High resolution 3D ultrasonic breast imaging by time-domain full waveform inversion. *Inverse Problems*, 38(2):Paper No. 025008, 39, 2022.

[29] F. Mainardi. *Fractional Calculus and Waves in Linear Viscoelasticity: An Introduction to Mathematical Models*. Imperial College Press, 2010.

[30] Alison E. Malcolm, Fernando Reitich, Jiaqi Yang, James F. Greenleaf, and Mostafa Fatemi. Numerical modeling for assessment and design of ultrasound vibro-acoustography systems. In *Biomedical Applications of Vibration and Acoustics for Imaging and Characterizations*. ASME Press, New York, 2007.

[31] Alison E. Malcolm, Fernando Reitich, Jiaqi Yang, James F. Greenleaf, and Mostafa Fatemi. A combined parabolic-integral equation approach to the acoustic simulation of vibro-acoustic imaging. *Ultrasonics*, 48:553–558, 2008.

[32] Jennifer L Mueller, Diego A C Cárdenas, and Sergio S Furuie. A preclinical simulation study of ultrasoundtomography for pulmonary bedside monitoring. In *Proceedings of the Second International Workshop on Medical Ultrasound Tomography (MUSTII)*, 2021.

[33] A Panfilova, RJG van Sloun, H Wijkstra, OA Sapozhnikov, and Mischi M. A review on b/a measurement methods with a clinical perspective. *The Journal of the Acoustical Society of America*, 149(4):2200, 2021.

[34] Uppal Talat. Tissue harmonic imaging. *Australas J Ultrasound Med*, 13(2):29–31, 2010.

[35] François Varray, Olivier Basset, Piero Tortoli, and Christian Cachard. Extensions of nonlinear b/a parameter imaging methods for echo mode. *IEEE transactions on ultrasonics, ferroelectrics, and frequency control*, 58:1232–44, 06 2011.

[36] Margaret G. Wismer. Finite element analysis of broadband acoustic pulses through inhomogenous media with power law attenuation. *The Journal of the Acoustical Society of America*, 120(6):3493–3502, 2006.

[37] Masahiro Yamamoto and Barbara Kaltenbacher. An inverse source problem related to acoustic nonlinearity parameter imaging. In Barbara Kaltenbacher, Anne Wald, and Thomas Schuster, editors, *Time-dependent Problems in Imaging and Parameter Identification*. Springer, New York, 2021.

[38] Dong Zhang, Xi Chen, and Xiu-fen Gong. Acoustic nonlinearity parameter tomography for biological tissues via parametric array from a circular piston source—theoretical analysis and computer simulations. *The Journal of the Acoustical Society of America*, 109(3):1219–1225, 2001.

[39] Dong Zhang, Xiufen Gong, and Shigong Ye. Acoustic nonlinearity parameter tomography for biological specimens via measurements of the second harmonics. *The Journal of the Acoustical Society of America*, 99(4):2397–2402, 1996.